C.P. No. 507
(21,392)
A.R.C. Technical Report

C.P. No. 507
(21,392)
A.R.C. Technical Report

MINISTRY OF AVIATION

AERONAUTICAL RESEARCH COUNCIL

CURRENT PAPERS

Wind Tunnel Measurements of Normal Force and Pitching Moment on Four Cone-Cylinder Combinations at Transonic and Supersonic Speeds

by

E. Huntley, B.Sc.

LONDON: HER MAJESTY'S STATIONERY OFFICE

1960

FOUR SHILLINGS NET

C.P. No.507

U.D.C. No. 533.696.3/4:533.6.011.35/5:533.6.013.13:533.6.013.15

Technical Note No. Aero 2621

May, 1959

ROYAL AIRCRAFT ESTABLISHMENT

WIND TUNNEL MEASUREMENTS OF NORMAL FORCE AND PITCHING MOMENT ON FOUR CONE-CYLINDER COMBINATIONS AT TRANSONIC AND SUPERSONIC SPEEDS

by

E. Huntley, B.Sc.

SUMMARY

Wind tunnel tests have been made, in the 3' × 3' tunnel at R.A.E. Bedford, on four cone-cylinder models at Mach numbers between 0.70 and 2.00. The tip of each cone was rounded and the overall fineness ratio of each model was less than 8.0.

The normal force and centre of pressure characteristics of the models (the datum for the latter being the cone-cylinder shoulder) were found to be dependent primarily on cone angle. The effect of increasing the tip radius from 0.20 to 0.50 times the body radius was negligible at all speeds.

LIST OF CONTENTS

LIST OF TABLES

LIST OF ILLUSTRATIONS

LIST OF ILLUSTRATIONS (Cont'd)

1 INTRODUCTION AND DETAILS OF MODEL

Information was required at transonic and supersonic speeds on the normal force and centre of pressure characteristics of cone-cylinder combinations of small fineness ratio. Tests were made, therefore, in the 3' × 3' tunnel at R.A.E. Bedford, on a model having a cylindrical body of 5.1 fineness ratio and four alternative nose shapes. These noses were conical with rounded tips and combined two values of tip radius with two values of cone semi-angle. These values are tabulated below and the general arrangement of the model is given in Fig.1.

Nose	Cone semi-angle	Tip radius / Body radius	Total fineness ratio
A	10°	0.20	7.5
B	10°	0.50	6.8
C	20°	0.20	6.3
D	20°	0.50	6.0

The sting on which the model was mounted incorporated a two component strain-gauge balance measuring normal force and pitching moment. It had a cylindrical section immediately downstream of the base of the model of length 7.6 inches (3.0 model calibres) and diameter 0.75 inches (0.3 model calibres) followed by a taper of 20° included angle.

2 TEST DETAILS

The model was tested at transonic speeds ($M = 0.70$ to 1.02) in the temporary transonic section[1] of the 3' × 3' tunnel and at $M = 1.42$ and 2.00 in the supersonic section[2].

The incidence range covered was from $\theta = -2^{\circ}$ to $+9^{\circ}$ at transonic speeds and from $\theta = -2^{\circ}$ to $+10^{\circ}$ at supersonic speeds.

At the time of the tests only half power was available so that the Reynolds numbers were half of those normally attained. A more recent check test at full power in the permanent transonic section gave results which compared very closely with the previous results so that the Reynolds number effect appears to be small. The Reynolds numbers of the tests, based on body diameter, are shown in Fig.2; they vary from 0.89×10^{6} at transonic speeds to 0.43×10^{6} at $M = 2.00$. In order to fix transition, a half inch wide band of carborundum powder mixed in aluminium paint was applied at the nose of each model.

It is estimated that the accuracy of the data is within the following limits:-

C_N	±0.003 ±0.004	$M < 2.00$ $M = 2.00$
C_m	±0.005 ±0.007	$M < 2.00$ $M = 2.00$
θ	±0.02	All M

These possible errors in C_N and C_m give rise to errors in the centre of pressure position, x_{cp}, which vary with incidence. The maximum error in x_{cp} (in terms of body calibres) is estimated to be ± 0.15 for incidences of 2-3 degrees, and to decrease to ± 0.05 as θ increases to 10°.

For $\theta > 2^{\circ}$, x_{cp} was obtained by dividing C_m by C_N; for $\theta = 0$ it was determined from the ratio of the mean slopes of the C_m v. θ and C_N v. θ curves as defined by the method of least squares for the experimental values between $\theta = \pm 2^{\circ}$ and the value of x_{cp} obtained for $\theta = 0$ is estimated to be more accurate than is suggested above. At supersonic speeds and at $M = 1.42$ in particular, there is some flow curvature in the tunnel giving rise to pitching moments at zero incidence. The effects of flow curvature were largely removed by displacing the curves to pass through the origin before obtaining the centre of pressure positions.

In the transonic regime the main tunnel interference effect is the delay (with increasing Mach number) of the rearward movement of the shock terminating the supersonic flow round the model shoulder. Since the effect only becomes noticeable above $M = 0.95$ results for Mach numbers up to and including $M = 0.95$ are believed to be accurate. Results for $M = 1.02$ are possibly less accurate but since the models were small (0.33% blockage) and short, the errors are again believed to be small.

3 PRESENTATION AND DISCUSSION OF RESULTS

All the results obtained from these tests are tabulated in Tables 1 to 4 and plotted in Figs.3 to 6 as curves of C_N v. θ and x_{cp} v. θ. Normal force curve slopes and centre of pressure positions at zero incidence are plotted against Mach number in Fig.7. Centre of pressure positions are given with the cone-cylinder shoulder as datum.

Results for Nose A (Fig.3) show that the variations with θ of C_N and x_{cp} are smooth at all Mach numbers. At transonic speeds the non-linear lift arising from the viscous cross flow over the body is small for the incidences covered in these tests and hence the centre of pressure variation with θ is also small. At supersonic speeds the non-linear lift is appreciably greater and the rearward movement of the centre of pressure with increase of incidence is correspondingly increased.

Results for Nose B (Fig.4) are very similar to the results for Nose A.

Fig.7, giving the variation with Mach number of the normal force curve slope and centre of pressure position at zero incidence shows that for both noses there is a slight transonic variation of $[dC_N/d\theta]_{\theta=0}$ followed by a gradual increase at supersonic speeds. The centre of pressure is just ahead of the shoulder of the model at transonic speeds, moves forward 0.6 to 0.7 calibres on increasing Mach number to 1.42 but moves back slightly for $M = 2.00$.

Results for Nose C (Fig.5) again show smooth variations of C_N and x_{cp} with θ but only for Mach numbers above 0.90. At $M = 0.90$, in particular, there is a sudden increase in C_N for $\theta = 7^{\circ}$ with a corresponding rearward movement of the centre of pressure. Fig.7(a) shows a 5% reduction in $[dC_N/d\theta]_{\theta=0}$ between $M = 0.80$ and 0.90 followed by a 28% increase as the Mach number increases to 2.00. The centre of pressure movement is also considerable (Fig.7(b)), particularly at transonic speeds, the difference in x_{cp} between $M = 0.80$ and 0.90 being 0.5 calibres.

Results for Nose D (Fig.6) are very similar to those for Nose C. It can be concluded, therefore, that the normal force and centre of pressure characteristics of these cone-cylinders are dependent on cone angle but independent of tip radius (for tip radii up to one half of the body radius).

The fairly considerable movements of the centre of pressure for noses C and D at transonic speeds, can be attributed to separation of the flow from the shoulder of the model. Schlieren photographs (Fig.8) taken in the solid-wall working section at an incidence of 6° and Mach numbers of approximately M = 0.88, 0.92 and 0.95 give a qualitative picture of what happens on the model in the slotted-wall section. When the free stream Mach number is sufficiently high a supersonic region forms round the shoulder of the model; the flow is over-expanded and is brought back to subsonic speeds again by a shock system consisting of an inclined shock followed by a normal shock. There is a range of incidence and Mach number within which boundary layer separation occurs. As the Mach number is increased the over-expansion and the shock system are modified and eventually, above some Mach number which depends on the incidence, fail to separate the boundary layer. The effects of the disappearance of the separation would be expected to include a decrease in normal force and a forward movement of the centre of pressure, as observed.

Consideration of the photographs and the centre of pressure movements with variation of incidence and Mach number suggests that with the model at zero incidence the flow is separated for Mach numbers around M = 0.80 but becomes attached on increasing Mach number to 0.90. For higher incidences the flow remains unattached to slightly higher Mach numbers but for all incidences the flow is attached for M = 0.95. Considering the results for M = 0.90, the flow is probably attached for $\theta = 0$ and up to $\theta = 6^\circ$. On increasing incidence to 8° the flow detaches and thus causes the increase in lift and the rearward movement of the centre of pressure.

The effect of Mach number on the non-linear lift can be seen in Figs.9 and 10. For a given incidence, the non-linear lift increases as the Mach number increases. Also, the incidence at which the non-linear lift commences, decreases as the Mach number is increased from M = 0.70 to 1.02 but remains approximately constant at 3 to 4° for supersonic Mach numbers up to 2.00.

4 CORRELATION WITH RESULTS FOR TRUE CONE-CYLINDERS AT SUPERSONIC SPEEDS

Since the results were found to be practically independent of cone tip radius, it seemed likely that they might correlate with data obtained from cone-cylinders with zero tip radius. In order to check this hypothesis values of normal force curve slope and centre of pressure position for zero incidence were obtained from charts in Ref.3. These charts are based on experimental results obtained for Mach numbers between 1.57 and 4.24 from a large range of models combining several values of cone included angle ($\leqslant 28^\circ$) with several body fineness ratios the results being correlated by the use of the Supersonic-Hypersonic Similarity parameter, $\beta d/\ell n$. It has to be noted that the results were obtained for a laminar boundary layer whereas for the present models the boundary layer is considered to have been turbulent. This should not, however, affect the comparison appreciably at zero incidence since the viscous effects are relatively unimportant at low incidences. The values obtained from these charts for (a) a 20° cone and (b) a 40° cone, each combined with a cylindrical body of 5.1 fineness ratio, are tabulated below together with the experimental results.

Configuration	$[dC_N/d\theta]_{\theta=0}$		$[x_{cp}]_{\theta=0}$	
	M = 1.41	M = 2.00	M = 1.41	M = 2.00
20° Cone	0.0464	0.0482	0.49	0.45
Exp. Nose A	0.0415	0.0458	0.77	0.55
Exp. Nose B	0.0418	0.0452	0.75	0.51
40° Cone	0.0512	0.0541	0.11	-0.02
Exp. Nose C	0.0441	0.0518	0.22	-0.07
Exp. Nose D	0.0442	0.0514	0.21	-0.07

At $M = 2.00$ the values of $[dC_N/d\theta]_{\theta=0}$ agree to within 4%, for both values of cone angle, but only to within 8% at $M = 1.42$. The centre of pressure positions also agree very well at $M = 2.00$ (to within 0.1 calibres for both values of cone angle) but not so well at $M = 1.41$ (within 0.3 calibres).

5 CONCLUSIONS

Wind tunnel tests have been made in the 3' x 3' tunnel at R.A.E. Bedford on four cone-cylinder combinations at Mach numbers between 0.70 and 2.00. Each model had a cylindrical body of 5.1 fineness ratio and the four alternative nose shapes were obtained by combining two values of tip radius with two values of cone angle.

It was found that the normal force and centre of pressure characteristics of these cone-cylinders (measured from the cone-cylinder shoulder) were dependent almost entirely on cone angle. The effect of increasing the tip radius from 0.20 to 0.50 times the body radius was negligible at all speeds.

Each 40° cone-cylinder showed considerable centre of pressure variation with Mach number at transonic speeds; these centre of pressure movements are attributed to flow separation from the shoulder of the model.

The results for $M = 2.00$ agreed very well with data from cone-cylinders, with zero tip radius, and correlated by the Supersonic-Hypersonic Similarity parameter, $\beta d/\ell n$. Values of $[dC_N/d\theta]_{\theta=0}$ agreed within 4% and centre of pressure positions within 0.1 calibres.

LIST OF SYMBOLS

$C_N = \frac{N}{qS}$	normal force coefficient
$C_m = \frac{m}{qSd}$	pitching moment coefficient. (Balance centre 1.69 calibres behind model shoulder.)
q	dynamic pressure
d	body diameter
S	body cross sectional area
ℓn	nose length
M	Mach number
cp	centre of pressure
x_{cp}	distance of centre of pressure ahead of model shoulder (in calibres)
θ	incidence
β	$\sqrt{M^2 - 1}$
$\frac{\beta d}{\ell n}$	Supersonic-Hypersonic similarity parameter

LIST OF REFERENCES

Ref. No.	Author	Title, etc.
1	Sutton, E. P.	The development of slotted working section liners for transonic operation of the N.A.E. 3-foot wind tunnel. R. and M. 3085, March, 1955.
2	Morris, D. E.	Calibration of the flow in the working section of the N.A.E. 3' x 3' tunnel. A.R.C. C.P. 261. September, 1954.
3	Dorrance, W. H. Norrell, R. G.	Correlation of cone-cylinder normal force and pitching moment data by the Hypersonic Similarity Rule. Jo. Ae. Sci. May, 1957.

TABLE 1

Results for Nose A

M	θ	C_N	C_m	x_{cp}
0.70	-1.95	-0.079	-0.149	+0.19
	-0.92	-0.040	-0.075	
	+0.10	+0.005	+0.006	0.14
	1.13	0.047	0.083	
	2.15	0.088	0.158	0.11
	3.17	0.131	0.236	0.10
	4.20	0.174	0.316	0.13
	5.22	0.216	0.397	0.15
	6.25	0.258	0.461	0.09
	7.27	0.305	0.542	0.08
	8.30	0.354	0.613	0.04
	9.32	0.403	0.678	-0.01
0.80	-1.95	-0.075	-0.147	+0.26
	-0.92	-0.036	-0.074	
	+0.10	+0.005	+0.006	0.18
	1.13	0.047	0.083	
	2.16	0.089	0.160	0.10
	3.18	0.131	0.238	0.14
	4.21	0.175	0.320	0.14
	5.24	0.217	0.396	0.13
	6.27	0.262	0.475	0.12
	7.29	0.307	0.548	0.10
	8.32	0.356	0.625	0.06
	9.35	0.408	0.684	-0.02
0.90	-1.95	-0.077	-0.152	+0.27
	-0.92	-0.037	-0.076	
	+0.10	+0.006	+0.005	0.16
	1.13	0.050	0.083	
	2.16	0.092	0.165	0.09
	3.19	0.134	0.246	0.15
	4.22	0.176	0.327	0.17
	5.25	0.220	0.407	0.16
	6.28	0.266	0.487	0.14
	7.31	0.314	0.561	0.10
	8.34	0.366	0.630	0.03
	9.38	0.424	0.693	-0.06

M	θ	C_N	C_m	x_{cp}
0.95	-1.96	-0.080	-0.158	+0.29
	-0.93	-0.037	-0.077	
	+0.10	+0.006	+0.006	0.22
	1.13	0.049	0.087	
	2.17	0.092	0.171	0.17
	3.20	0.136	0.254	0.18
	4.23	0.179	0.337	0.20
	5.26	0.225	0.417	0.16
	6.29	0.273	0.497	0.13
	7.33	0.325	0.569	0.06
	8.36	0.381	0.641	-0.01
	9.40	0.444	0.704	-0.11
1.02	-1.96	-0.081	-0.170	+0.40
	-0.93	-0.036	-0.081	
	+0.10	+0.007	+0.007	0.31
	1.13	0.051	0.096	
	2.17	0.096	0.184	0.23
	3.20	0.140	0.275	0.27
	4.23	0.187	0.361	0.25
	5.26	0.236	0.447	0.20
	6.29	0.284	0.532	0.18
	7.33	0.335	0.615	0.15
	8.36	0.393	0.696	0.08
	9.40	0.455	0.774	0.01
1.42	-1.91	-0.080	-0.194	+0.73
	-0.89	-0.036	-0.091	
	+0.14	+0.005	+0.011	0.77
	1.17	0.048	0.120	
	2.20	0.091	0.225	0.78
	3.23	0.135	0.318	0.66
	4.25	0.182	0.414	0.58
	5.28	0.232	0.513	0.52
	6.32	0.288	0.608	0.42
	7.35	0.345	0.702	0.35
	8.38	0.409	0.786	0.23
	9.41	0.477	0.862	0.11
	10.45	0.559	0.965	0.04
2.00	-1.90	-0.088	-0.182	+0.39
	-0.89	-0.042	-0.090	
	+0.14	+0.007	+0.016	0.55
	1.16	0.053	0.118	
	2.18	0.099	0.236	0.69
	3.20	0.052	0.331	0.50
	4.22	0.204	0.417	0.36
	5.24	0.260	0.522	0.32
	6.27	0.322	0.613	0.21
	7.29	0.393	0.711	0.12
	8.32	0.470	0.782	-0.03
	9.35	0.563	0.859	-0.17
	10.37	0.665	0.917	-0.31

TABLE 2

Results for Nose B

M	θ	C_N	C_m	x_{cp}
0.70	-0.94	-0.077	-0.140	+0.13
	-0.92	-0.038	-0.067	
	+0.10	+0.003	+0.005	0.07
	1.12	0.042	0.073	
	2.15	0.087	0.150	0.03
	3.17	0.129	0.225	0.05
	4.20	0.171	0.297	0.04
	5.22	0.215	0.374	0.05
	6.25	0.262	0.448	0.02
	7.27	0.304	0.512	-0.01
	8.29	0.352	0.582	-0.04
	19.32	0.399	0.656	-0.05
0.80	-1.95	-0.082	-0.142	+0.03
	-0.92	-0.037	-0.068	
	+0.10	+0.002	+0.002	0.04
	1.13	0.046	0.077	
	2.15	0.087	0.152	0.15
	3.18	0.127	0.225	0.08
	4.21	0.173	0.305	0.07
	5.24	0.214	0.379	0.08
	6.26	0.263	0.453	0.04
	7.29	0.304	0.522	0.03
	8.32	0.353	0.588	-0.03
	9.34	0.403	0.650	-0.08
0.90	-1.96	-0.083	-0.145	+0.05
	-0.93	-0.040	-0.066	
	+0.10	+0.006	+0.008	0.03
	1.13	0.047	0.080	
	2.16	0.090	0.155	0.03
	3.19	0.132	0.233	0.07
	4.22	0.174	0.313	0.11
	5.25	0.218	0.389	0.09
	6.28	0.264	0.465	0.08
	7.31	0.311	0.539	0.04
	8.34	0.365	0.611	-0.02
	9.37	0.420	0.668	-0.10
0.95	-1.90	-0.082	-0.150	+0.15
	-0.93	-0.040	-0.076	
	+0.10	+0.004	+0.004	0.13
	1.13	0.047	0.083	
	2.16	0.089	0.161	0.12
	3.19	0.133	0.245	0.15
	4.23	0.177	0.323	0.13
	5.26	0.222	0.405	0.13
	6.29	0.273	0.479	0.06
	7.32	0.323	0.549	0.01
	8.36	0.381	0.620	-0.07
	9.39	0.444	0.688	-0.14
1.02	-1.96	-0.081	-0.168	+0.37
	-0.93	-0.040	-0.079	
	+0.10	+0.004	+0.006	0.35
	1.13	0.045	0.092	
	2.16	0.088	0.178	0.34
	3.19	0.134	0.266	0.29
	4.22	0.181	0.349	0.24
	5.26	0.229	0.433	0.20
	6.29	0.280	0.512	0.14
	7.32	0.333	0.595	0.09
	8.36	0.391	0.679	0.05
	9.39	0.452	0.749	-0.04
1.42	-1.91	-0.081	-0.186	+0.60
	-0.89	-0.037	-0.095	
	+0.14	+0.006	+0.018	0.75
	1.17	0.048	0.122	
	2.20	0.092	0.219	0.70
	3.23	0.138	0.319	0.63
	4.25	0.186	0.410	0.51
	5.28	0.236	0.509	0.47
	6.31	0.291	0.601	0.38
	7.35	0.349	0.696	0.30
	8.38	0.413	0.785	0.21
	9.41	0.485	0.865	0.09
	10.45	0.567	0.973	0.03
2.00	-1.90	-0.087	-0.186	+0.45
	-0.88	-0.039	-0.088	
	+0.14	+0.005	+0.020	0.51
	1.16	0.052	0.119	
	2.18	0.098	0.217	0.52
	3.20	0.147	0.313	0.44
	4.22	0.200	0.403	0.33
	5.24	0.256	0.480	0.19
	6.26	0.317	0.568	0.10
	7.29	0.384	0.665	0.04
	8.31	0.459	0.734	-0.09
	9.34	0.550	0.800	-0.24
	10.37	0.654	0.848	-0.39

TABLE 3

Results for Nose C

M	θ	C_N	C_m	x_{cp}
0.70	-1.94	-0.079	-0.094	-0.50
	-0.92	-0.036	-0.043	
	+0.10	+0.004	+0.006	-0.49
	1.12	0.046	0.055	
	2.14	0.089	0.106	-0.50
	3.16	0.132	0.153	-0.53
	4.18	0.177	0.208	-0.52
	5.20	0.215	0.262	-0.47
	6.23	0.262	0.316	-0.48
	7.25	0.303	0.368	-0.48
	8.27	0.354	0.415	-0.52
	9.29	0.395	0.457	-0.53
0.80	-1.94	-0.083	-0.069	-0.86
	-0.92	-0.038	-0.028	
	+0.10	+0.007	+0.011	-0.88
	1.12	0.047	0.033	
	2.14	0.091	0.077	-0.85
	3.17	0.133	0.124	-0.76
	4.19	0.177	0.175	-0.70
	5.21	0.224	0.227	-0.68
	6.24	0.267	0.279	-0.65
	7.26	0.314	0.329	-0.64
	8.29	0.363	0.377	-0.65
	9.31	0.409	0.416	-0.67
0.90	-1.95	-0.078	-0.108	-0.31
	-0.92	-0.037	-0.053	
	+0.10	+0.006	+0.004	-0.34
	1.13	0.046	0.060	
	2.15	0.088	0.117	-0.36
	3.18	0.131	0.174	-0.37
	4.20	0.173	0.229	-0.37
	5.23	0.214	0.283	-0.37
	6.25	0.260	0.339	-0.39
	6.77	0.294	0.331	-0.56
	7.28	0.326	0.340	-0.65
	8.30	0.381	0.361	-0.74
	9.33	0.438	0.379	-0.83

M	∂	C_N	C_m	x_{cp}
0.95	-1.95	-0.079	-0.125	-0.12
	-0.92	-0.037	-0.060	
	+0.10	+0.004	+0.005	-0.12
	1.13	0.046	0.071	
	2.16	0.086	0.134	-0.14
	3.19	0.131	0.202	-0.15
	4.23	0.174	0.265	-0.17
	5.24	0.219	0.328	-0.20
	6.27	0.266	0.383	-0.25
	7.30	0.314	0.436	-0.30
	8.32	0.368	0.470	-0.41
	9.35	0.426	0.503	-0.51
1.02	-1.95	-0.081	-0.148	+0.13
	-0.93	-0.039	-0.075	
	+0.10	+0.004	+0.007	0.13
	1.13	0.046	0.085	
	2.16	0.089	0.160	0.10
	3.19	0.132	0.236	0.10
	4.22	0.176	0.311	0.08
	5.25	0.223	0.384	0.03
	6.28	0.272	0.451	-0.03
	7.31	0.324	0.518	-0.09
	8.34	0.380	0.582	-0.16
	9.37	0.439	0.648	-0.22
1.42	-1.93	-0.084	-0.163	+0.25
	-0.92	-0.039	-0.077	
	+0.12	+0.007	+0.011	0.22
	1.15	0.051	0.098	
	2.17	0.097	0.182	0.19
	3.20	0.143	0.261	0.13
	4.23	0.192	0.344	0.10
	5.25	0.243	0.422	0.05
	6.28	0.298	0.496	-0.03
	7.31	0.355	0.570	-0.09
	8.34	0.417	0.637	-0.16
	9.37	0.484	0.697	-0.25
	10.40	0.562	0.755	-0.35
2.00	-1.92	-0.101	-0.162	-0.09
	-0.90	-0.046	-0.077	
	+0.12	+0.005	+0.007	-0.07
	1.14	0.058	0.097	
	2.16	0.111	0.179	-0.08
	3.18	0.167	0.242	-0.24
	4.20	0.225	0.338	-0.19
	5.22	0.285	0.412	-0.24
	6.24	0.350	0.479	-0.32
	7.26	0.421	0.549	-0.38
	8.29	0.499	0.606	-0.48
	9.31	0.590	0.644	-0.60
	10.34	0.678	0.662	-0.71

TABLE 4

Results for Nose D

M	θ	C_N	C_m	x_{cp}
0.70	-1.94	-0.082	-0.091	-0.58
	-0.92	-0.040	-0.045	
	+0.10	+0.002	+0.005	-0.57
	1.12	0.045	0.051	
	2.14	0.089	0.101	-0.56
	3.16	0.131	0.150	-0.55
	4.18	0.170	0.201	-0.51
	5.20	0.217	0.252	-0053
	6.22	0.258	0.302	-0.52
	7.25	0.306	0.354	-0.54
	8.27	0.352	0.402	-0.55
	9.29	0.396	0.445	-0.57
0.80	-1.94	-0.084	-0.065	-0.92
	-0.92	-0.040	-0.033	
	+0.10	+0.003	+0.001	-0.90
	1.12	0.050	0.035	
	2.14	0.089	0.074	-0.86
	3.17	0.131	0.120	-0.77
	4.19	0.177	0.168	-0.74
	5.21	0.221	0.218	-0.71
	6.24	0.264	0.268	-0.67
	7.26	0.315	0.320	-0.68
	8.28	0.358	0.365	-0.67
	9.31	0.410	0.406	-0.70
0.90	-1.95	-0.079	-0.104	-0.37
	-0.92	-0.038	-0.051	
	+0.10	+0.004	+0.004	-0.40
	1.13	0.045	0.056	
	2.17	0.088	0.111	-0.43
	3.18	0.128	0.165	-0.40
	4.20	0.172	0.220	-0.41
	5.23	0.215	0.276	-0.41
	6.25	0.261	0.325	-0.45
	7.28	0.318	0.351	-0.59
	8.31	0.378	0.379	-0.69
	9.33	0.434	0.405	-0.76
0.95	-1.95	-0.081	-0.123	-0.17
	-0.93	-0.038	-0.059	
	+0.10	+0.006	+0.004	-0.16
	1.13	0.043	0.067	
	2.16	0.085	0.130	-0.17
	3.18	0.129	0.193	-0.19
	4.21	0.172	0.256	-0.20
	5.24	0.216	0.320	-0.21
	6.27	0.263	0.371	-0.28
	7.30	0.314	0.423	-0.34
	8.32	0.367	0.455	-0.45
	9.35	0.425	0.485	-0.55
1.02	-1.95	-0.080	-0.144	+0.10
	0.92	-0.038	-0.071	
	+0.10	+0.003	+0.004	0.09
	1.13	0.047	0.083	
	2.16	0.088	0.156	0.09
	3.19	0.131	0.229	0.06
	4.22	0.176	0.303	0.03
	5.25	0.222	0.378	0.01
	6.27	0.273	0.440	-0.08
	7.30	0.325	0.507	-0.13
	8.34	0.381	0.576	-0.18
	9.37	0.440	0.635	-0.25
1.42	-1.93	-0.086	-0.162	+0.20
	-0.91	-0.039	-0.078	
	+0.12	+0.006	+0.010	0.21
	1.15	0.050	0.099	
	2.17	0.097	0.182	0.19
	3.20	0.144	0.264	0.15
	4.23	0.192	0.342	0.09
	5.25	0.243	0.418	0.03
	6.28	0.299	0.493	-0.04
	7.31	0.356	0.564	-0.11
	8.34	0.421	0.633	-0.19
	9.37	0.489	0.693	-0.27
	10.40	0.571	0.745	-0.39
2.00	-1.92	-0.099	-0.161	-0.07
	-0.90	-0.046	-0.074	
	+0.12	+0.007	+0.008	-0.07
	1.14	0.058	0.097	
	2.16	0.111	0.179	-0.09
	3.18	0.167	0.253	-0.17
	4.20	0.224	0.326	-0.23
	5.22	0.281	0.383	-0.33
	6.24	0.342	0.454	-0.37
	7.26	0.411	0.512	-0.45
	8.28	0.488	0.562	-0.54
	9.30	0.576	0.599	-0.65
	10.33	0.678	0.610	-0.79

WT.2078.C.P.507.K3 - Printed in England.

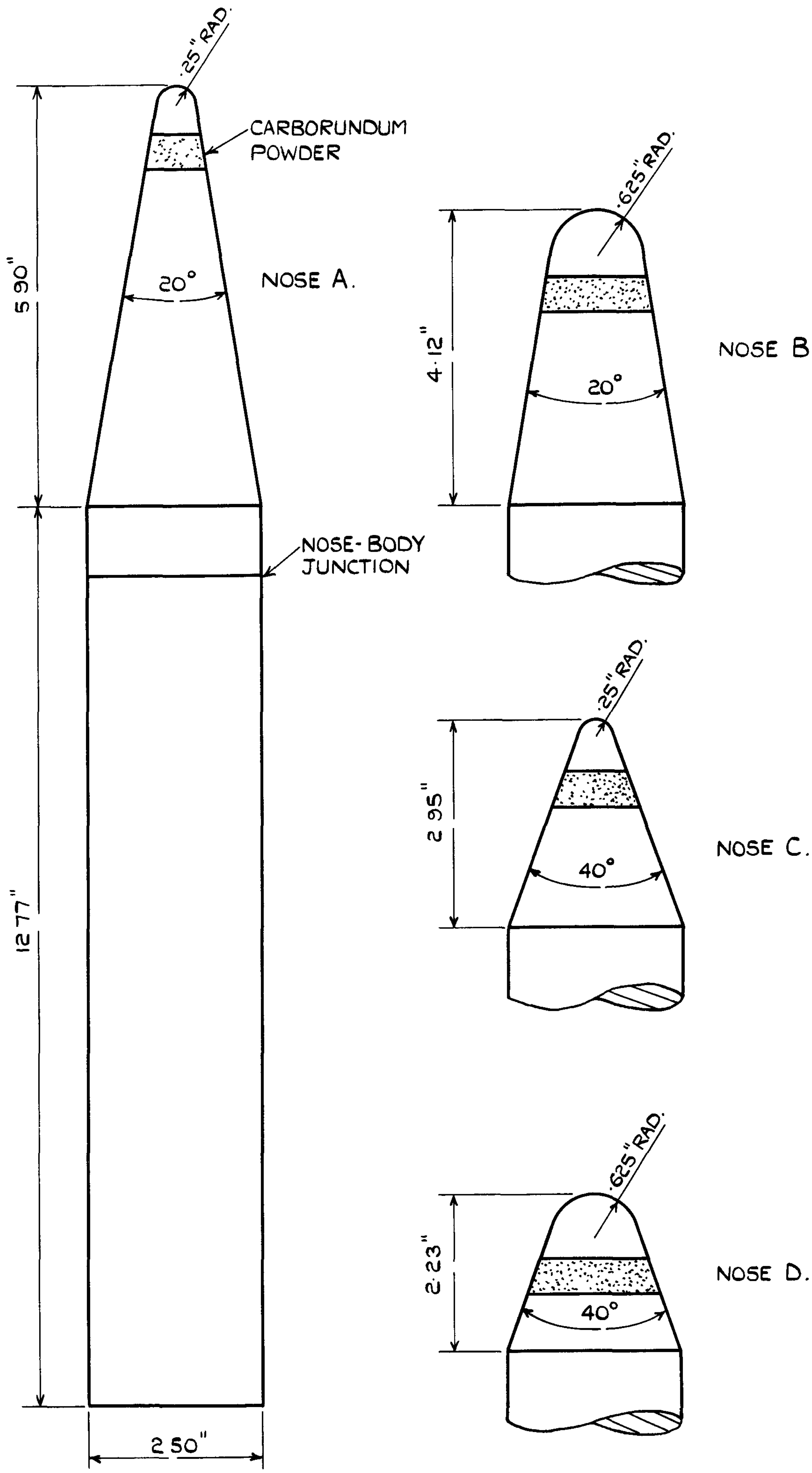

FIG. 1. MODEL DETAILS.

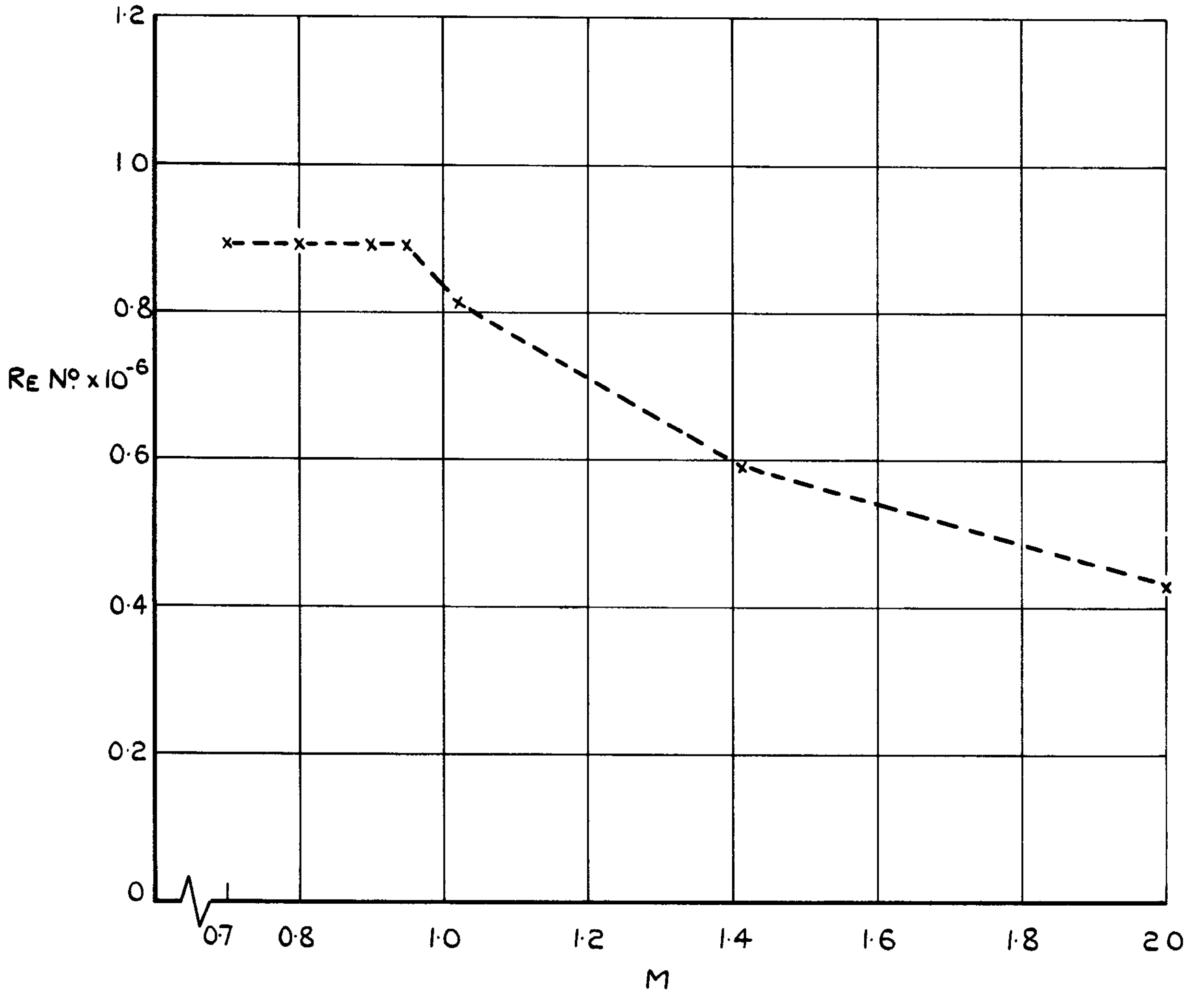

FIG. 2. VARIATION OF TEST REYNOLDS NUMBER WITH MACH NUMBER.

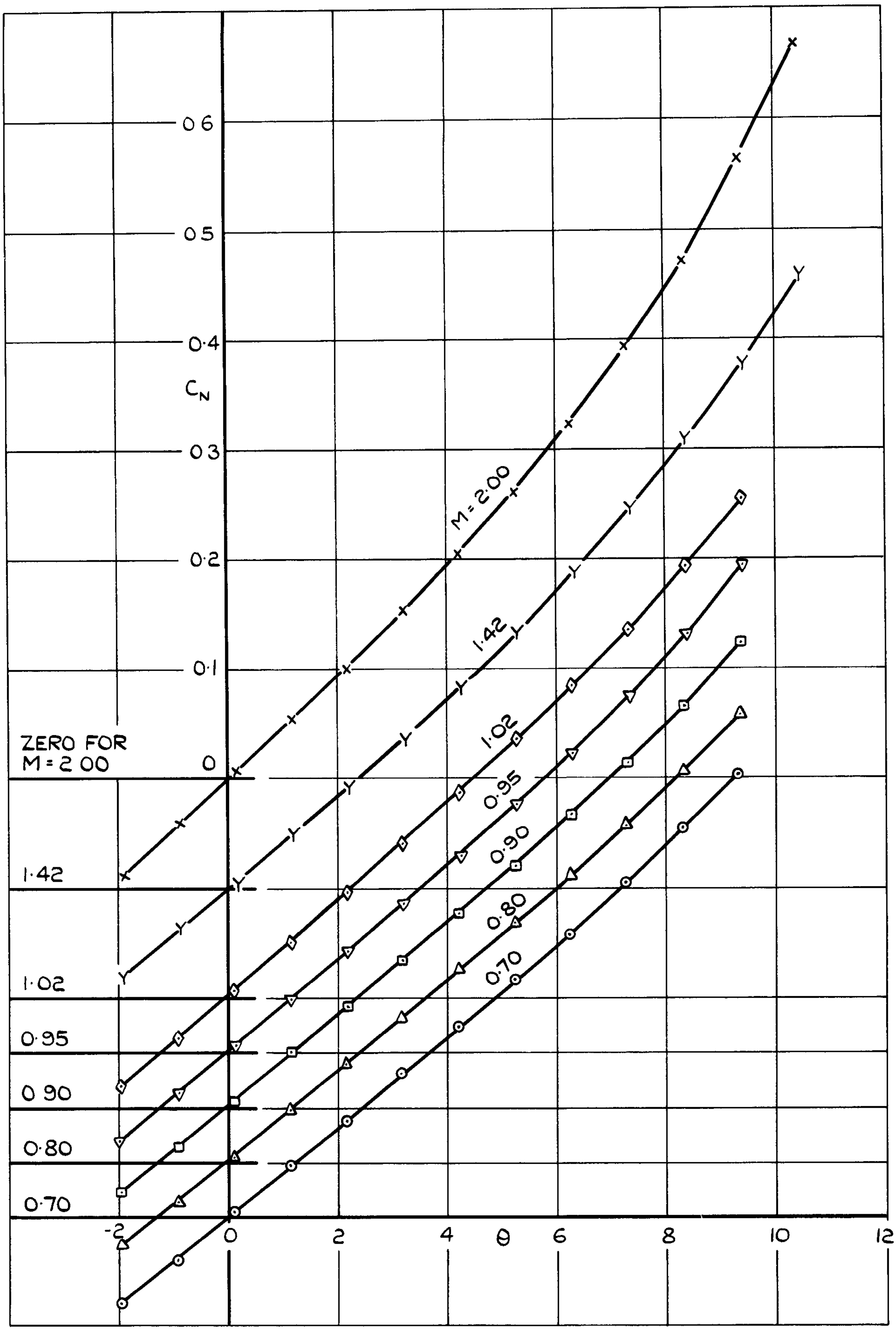

FIG. 3 (a) VARIATION OF C_N WITH θ FOR NOSE A.

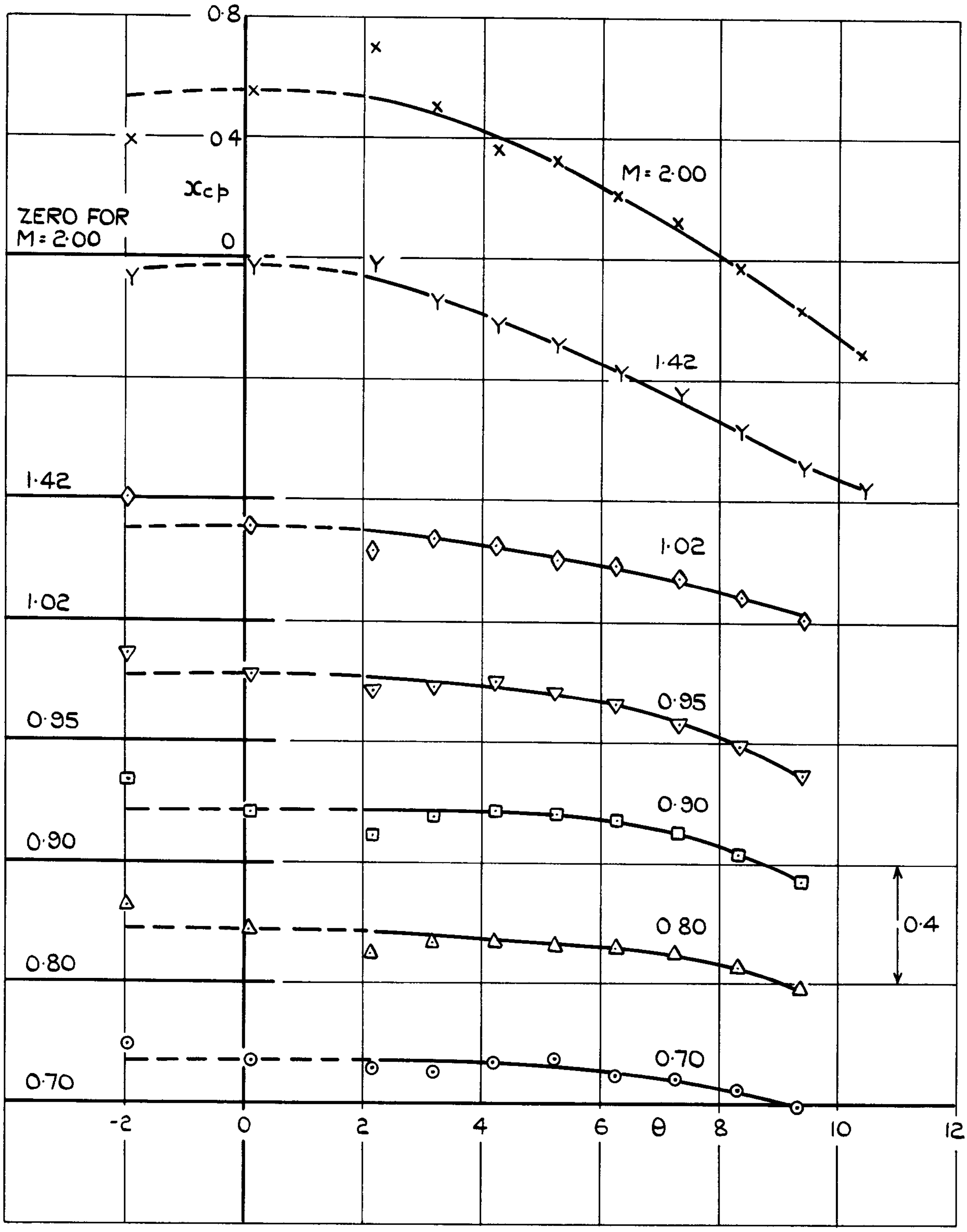

FIG. 3 (b) VARIATION OF $x_{c.p.}$ WITH θ FOR NOSE A.

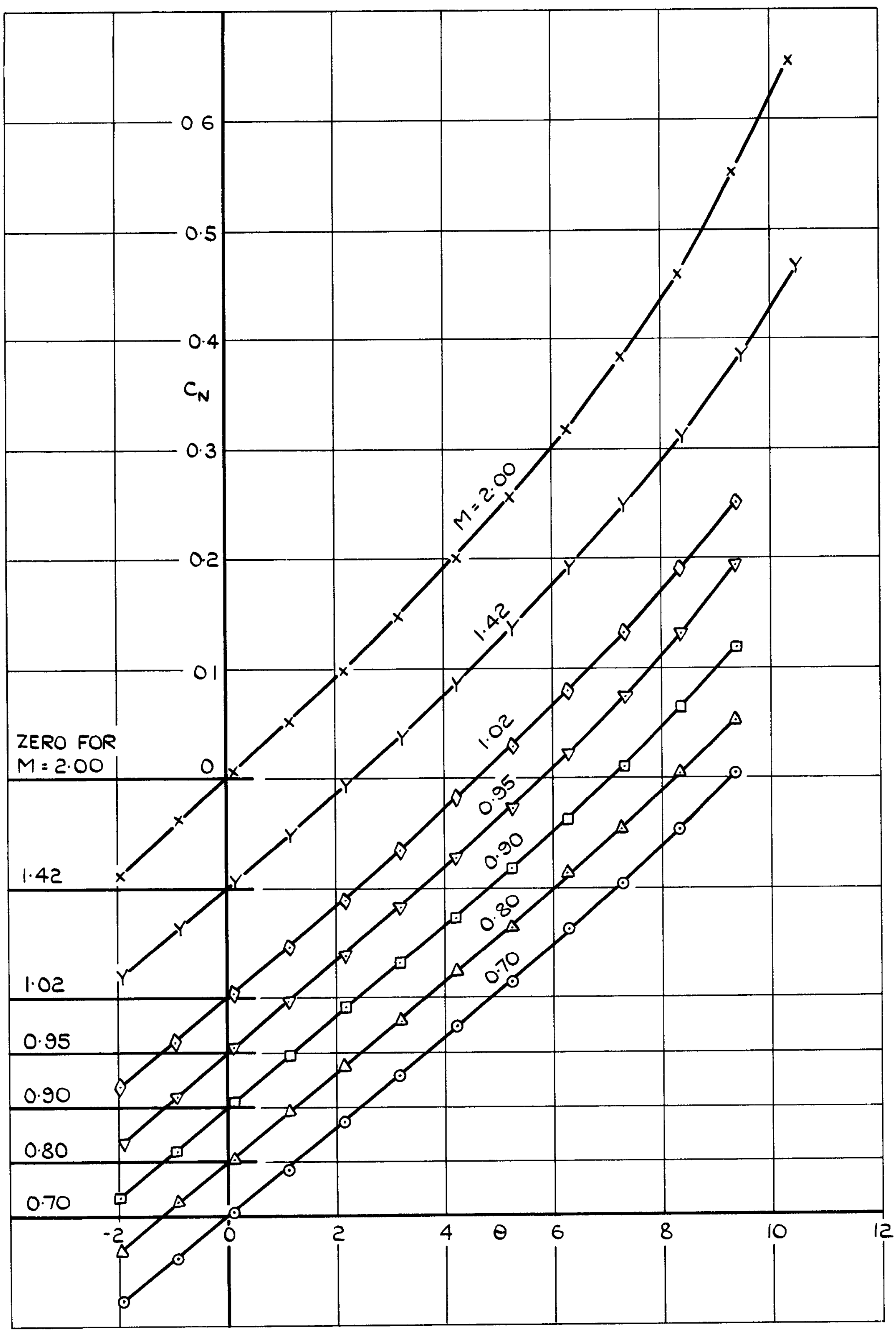

FIG. 4 (a) VARIATION OF C_N WITH θ FOR NOSE B.

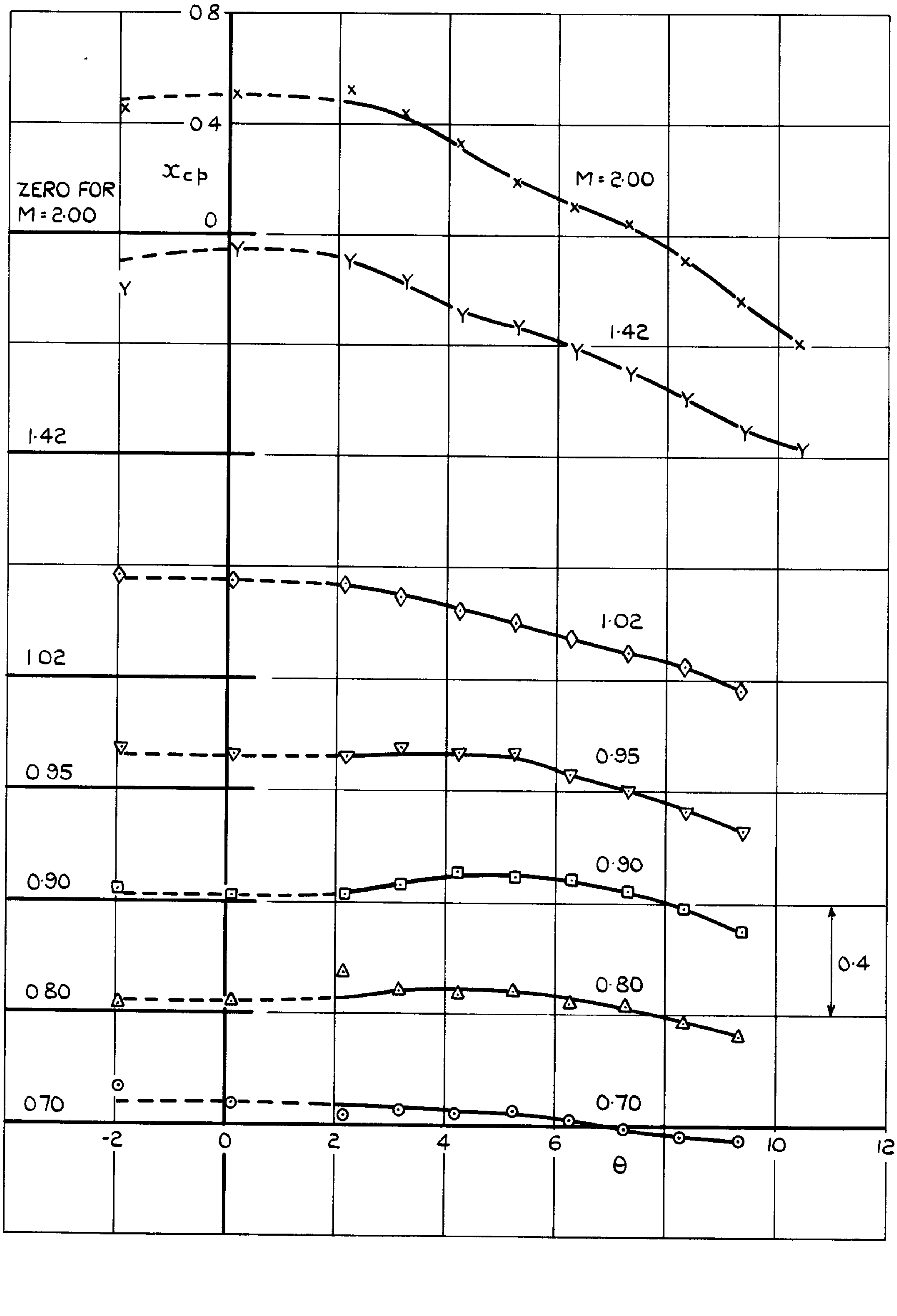

FIG. 4 (b) VARIATION OF $x_{c.p.}$ WITH θ FOR NOSE B.

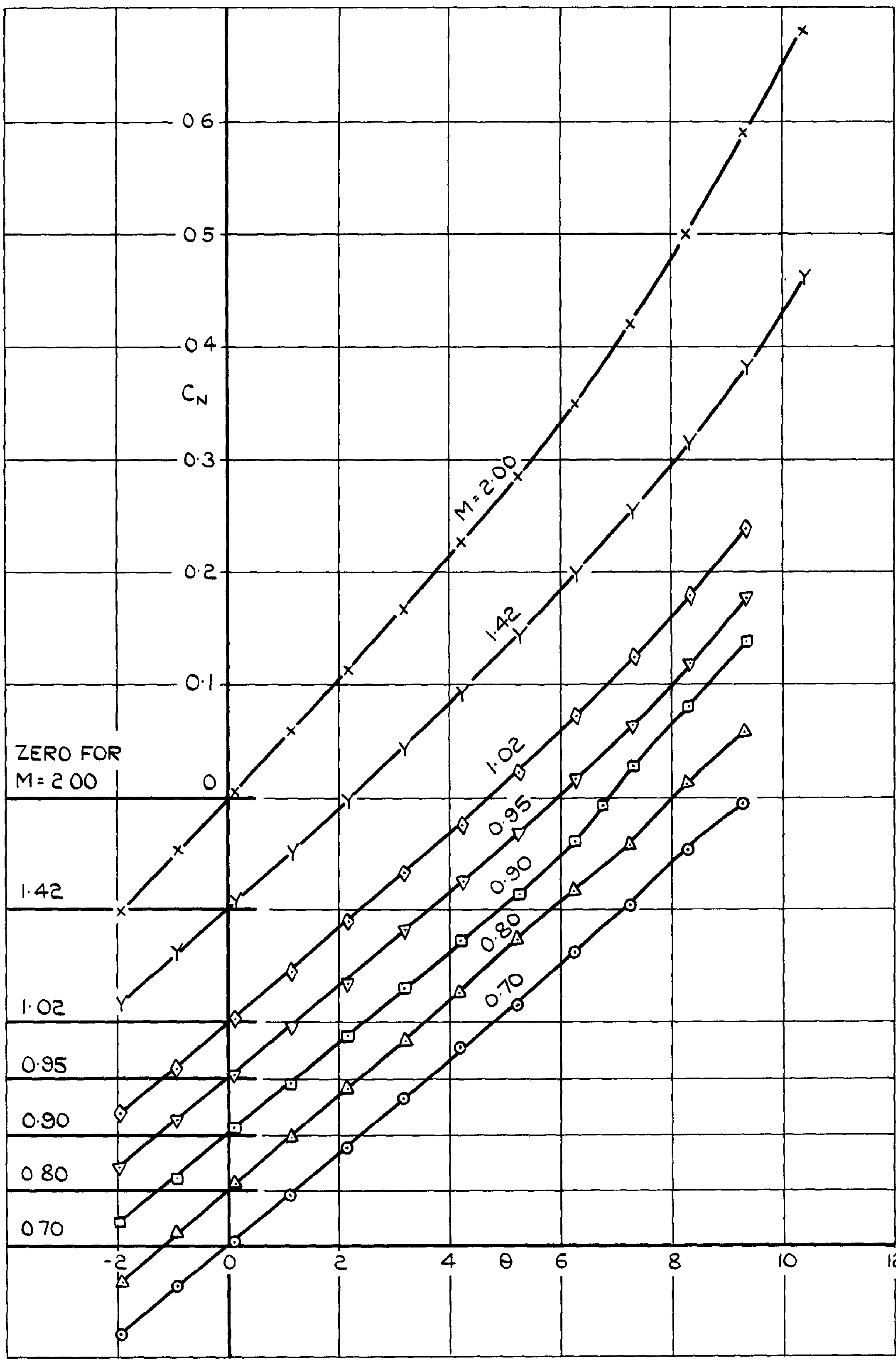

FIG. 5 (a) VARIATION OF C_N WITH θ FOR NOSE C.

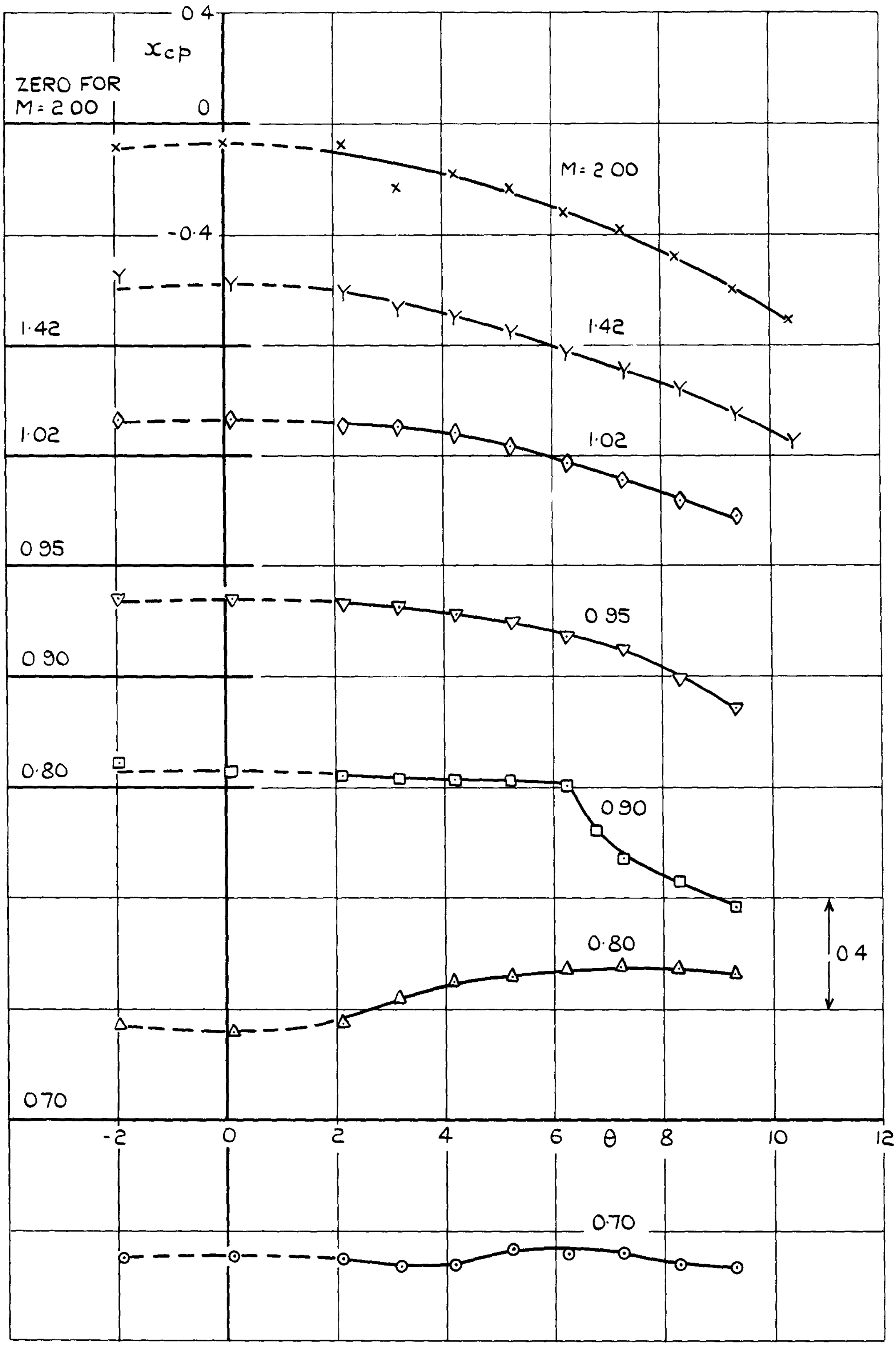

FIG. 5 (b) VARIATION OF x_{cp} WITH θ FOR NOSE C.

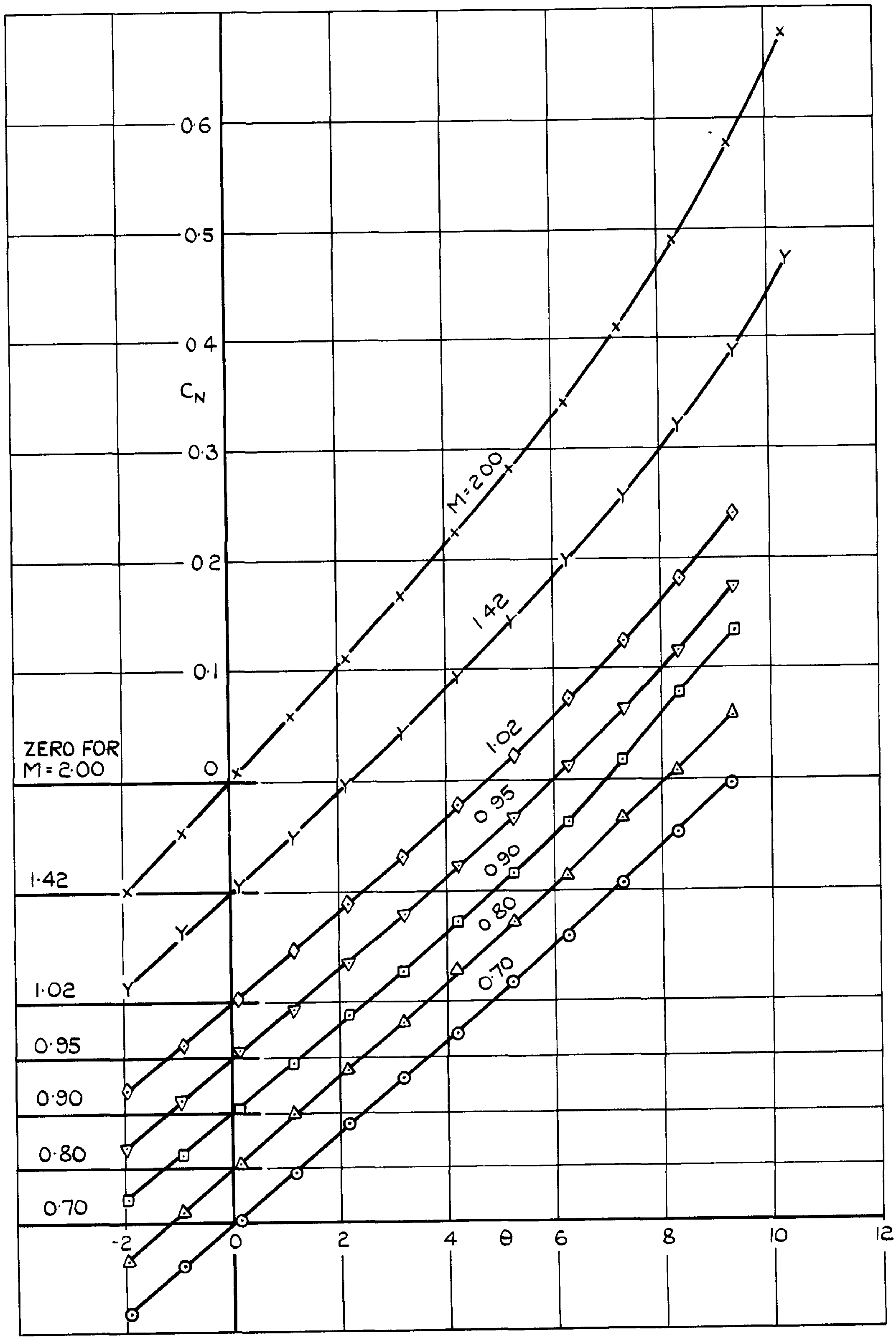

FIG. 6 (a) VARIATION OF C_N WITH θ FOR NOSE D.

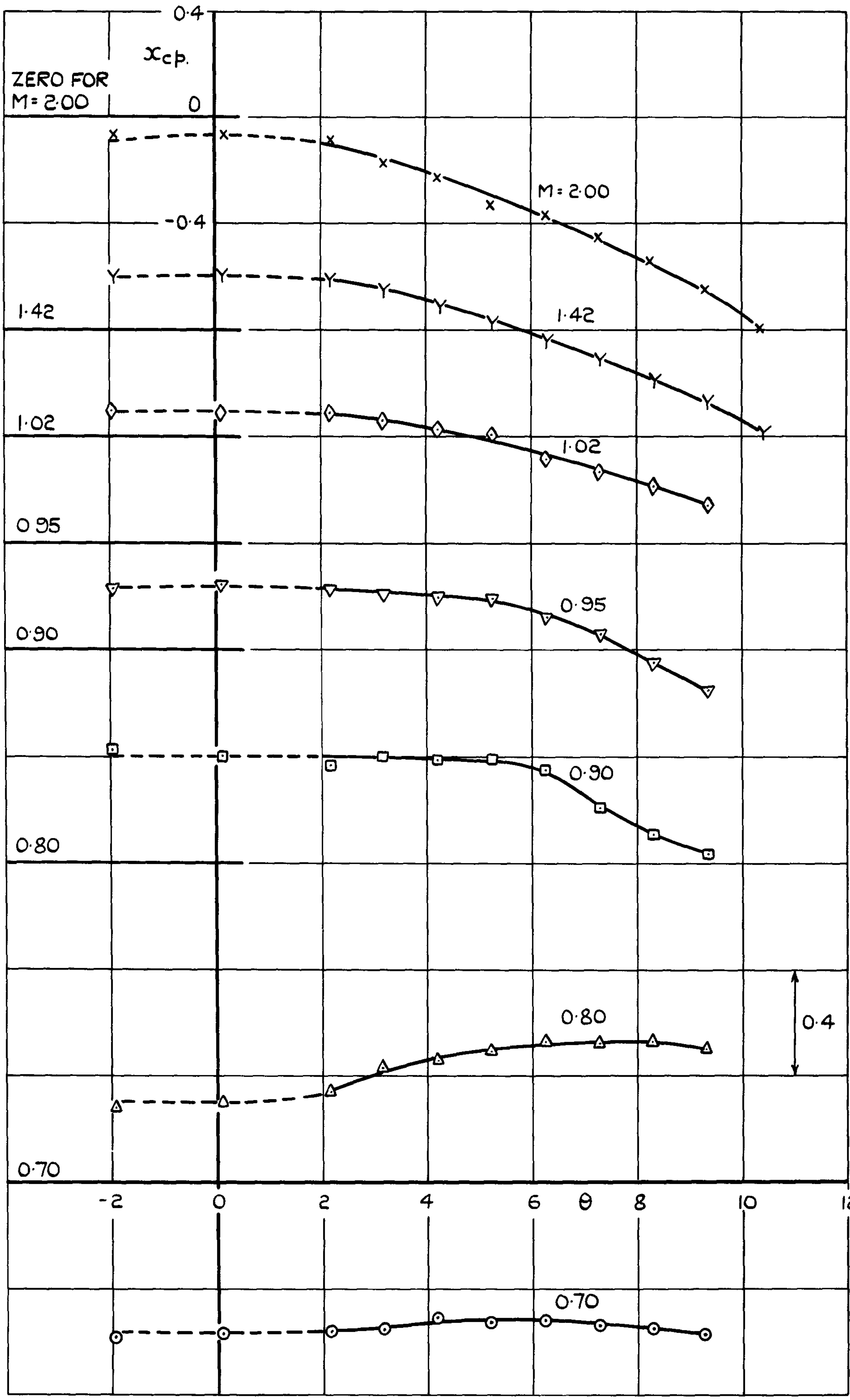

FIG. 6(b) VARIATION OF $x_{c.p.}$ WITH θ FOR NOSE D.

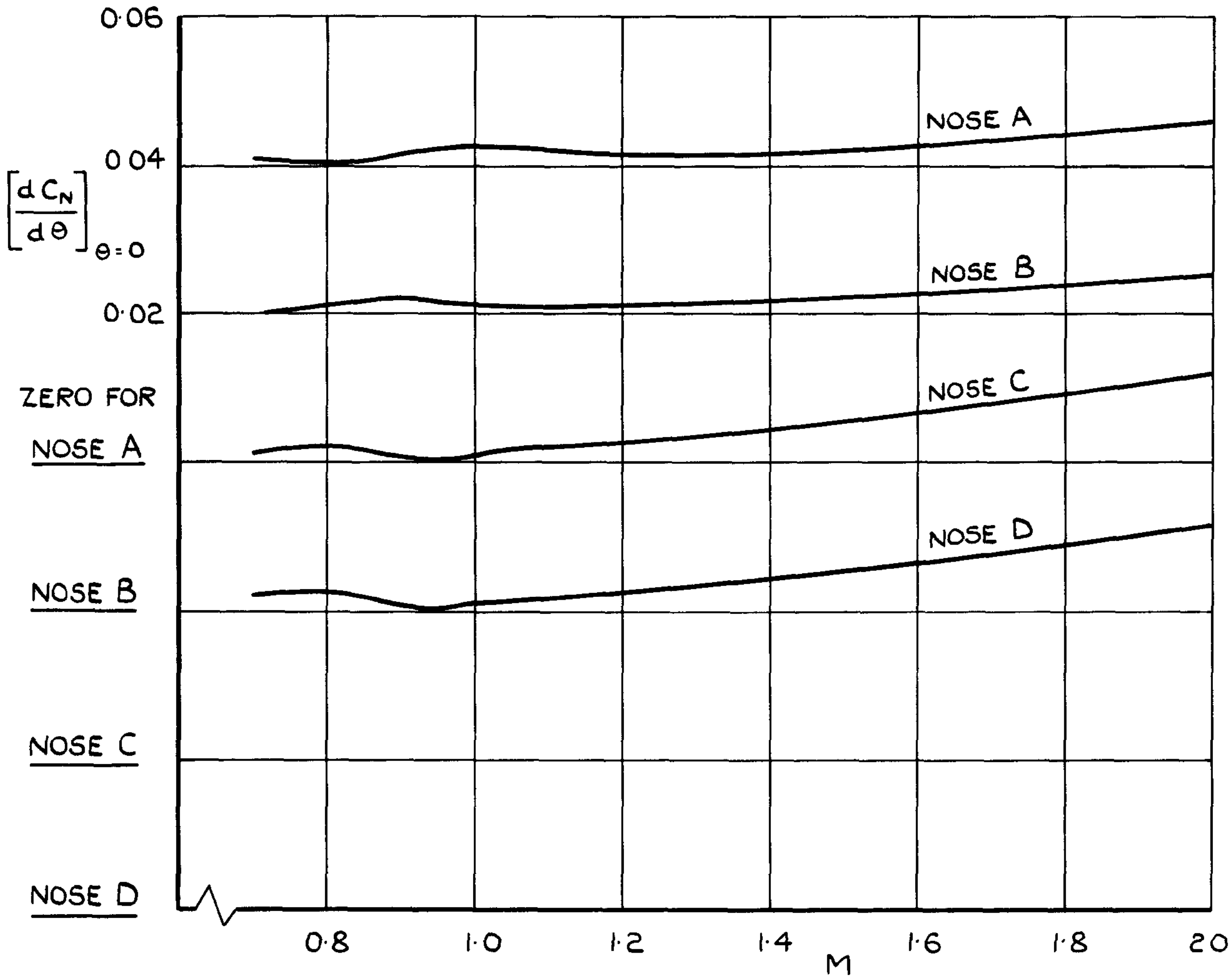

FIG. 7(a) VARIATION WITH MACH NUMBER OF NORMAL FORCE CURVE SLOPE AT ZERO INCIDENCE.

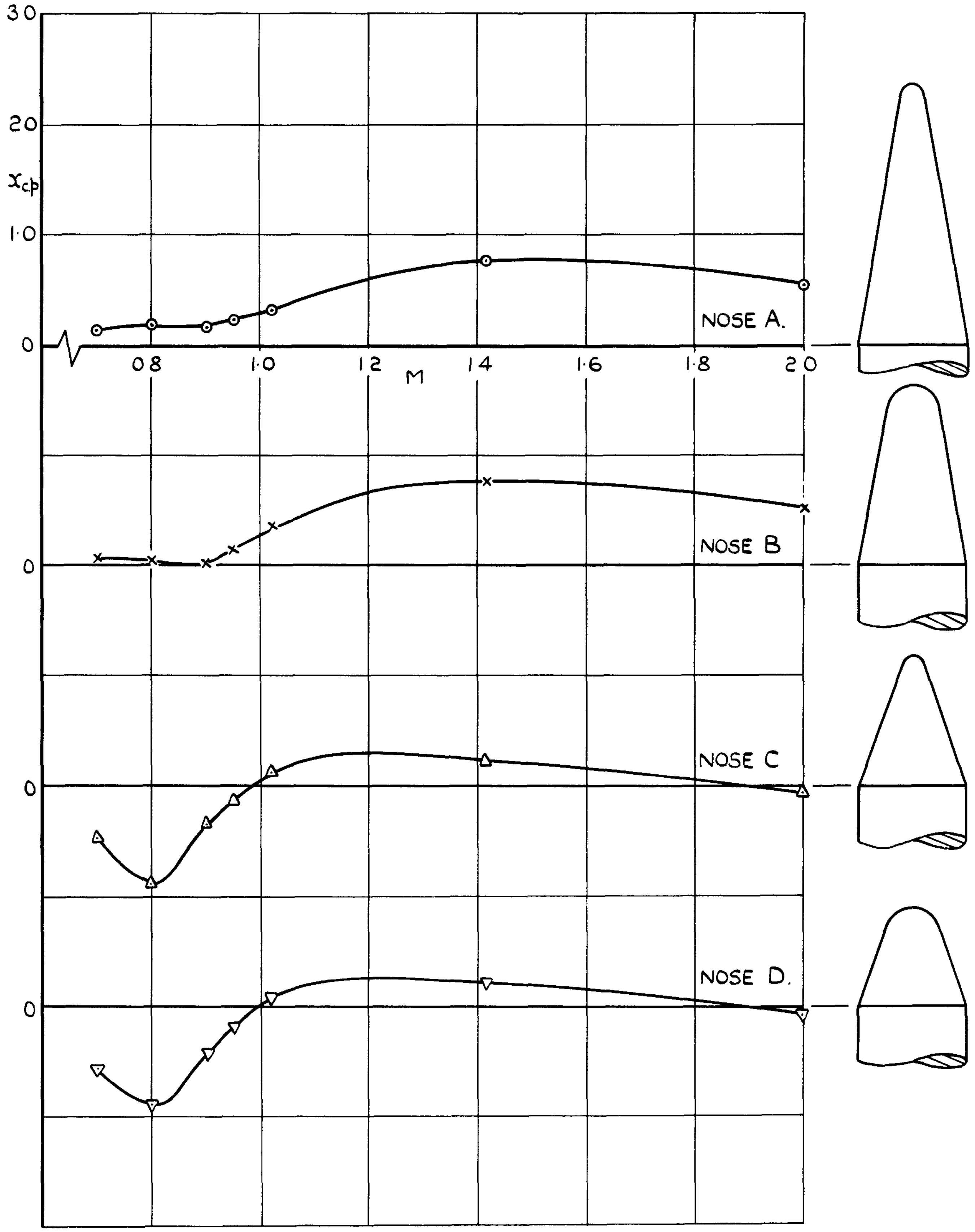

FIG.7(b) VARIATION WITH MACH NUMBER OF THE CENTRE OF PRESSURE POSITION AT ZERO INCIDENCE.

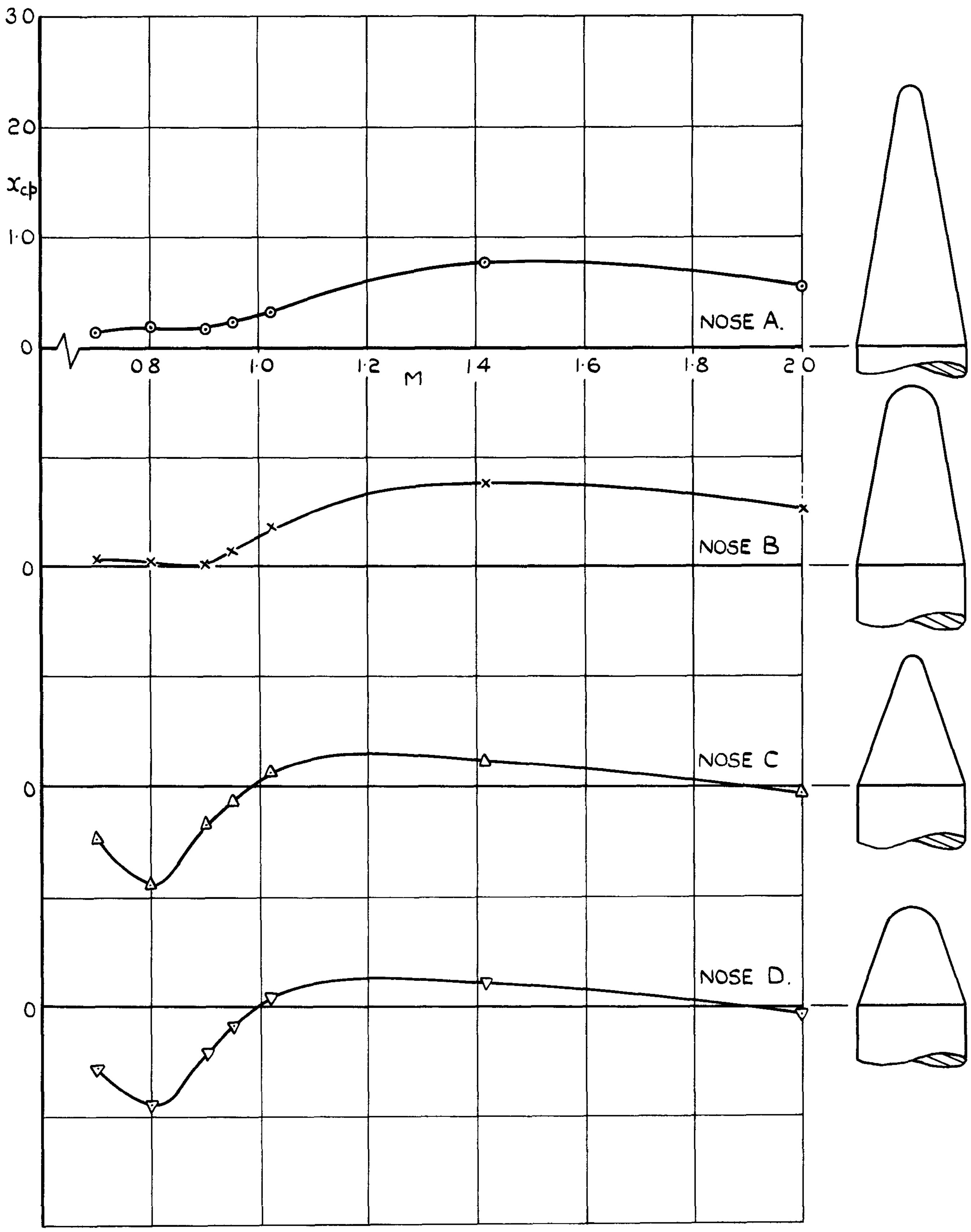

FIG.7(b) VARIATION WITH MACH NUMBER OF THE CENTRE OF PRESSURE POSITION AT ZERO INCIDENCE.

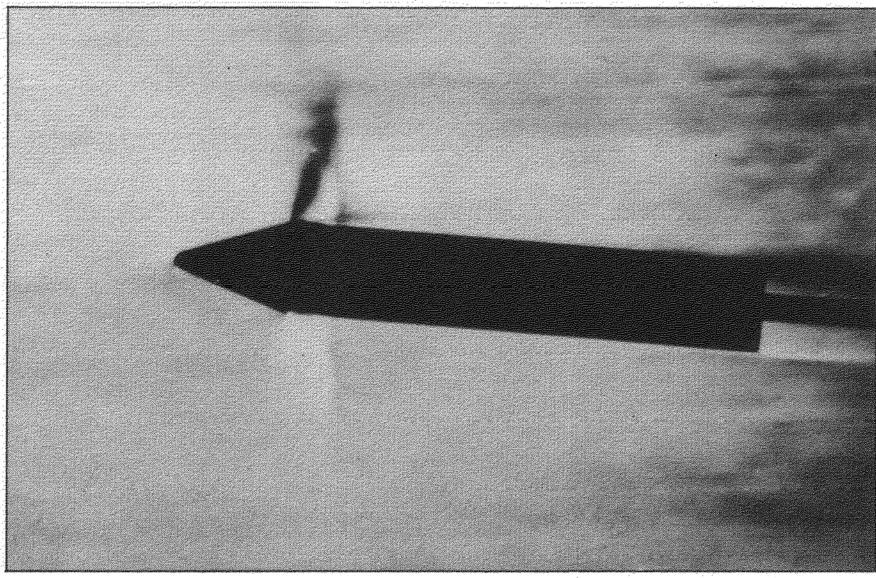

M $\doteqdot$ 0.88

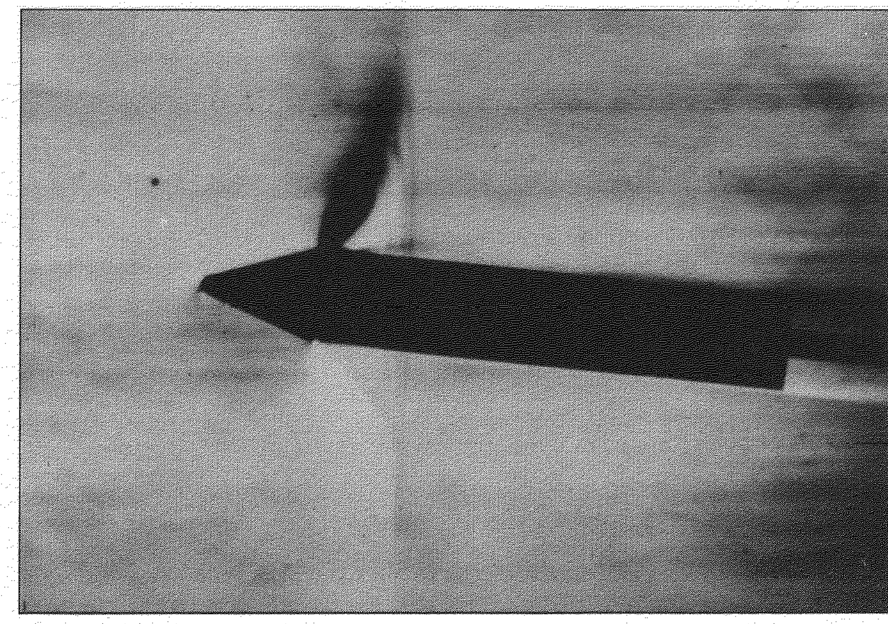

M $\doteqdot$ 0.92

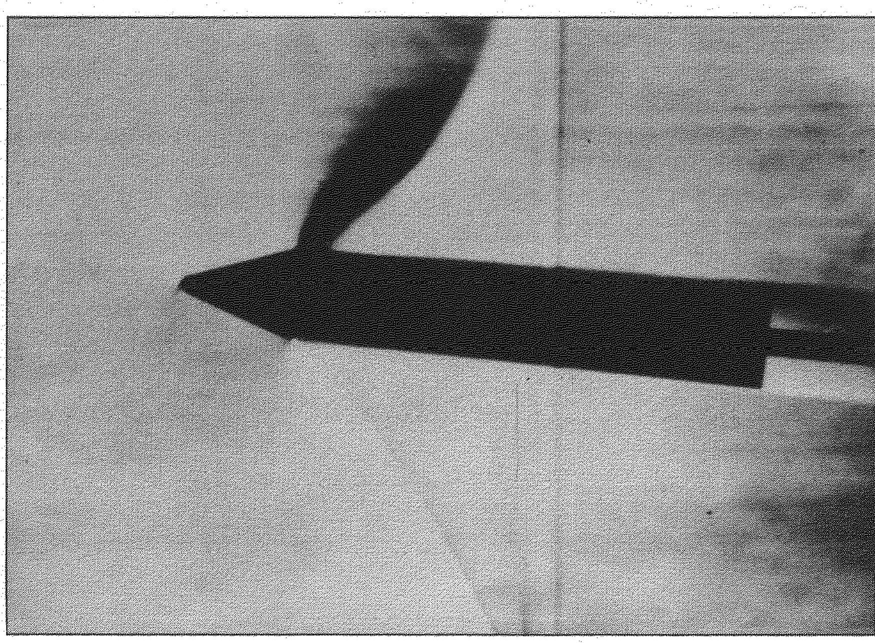

M $\doteqdot$ 0.95

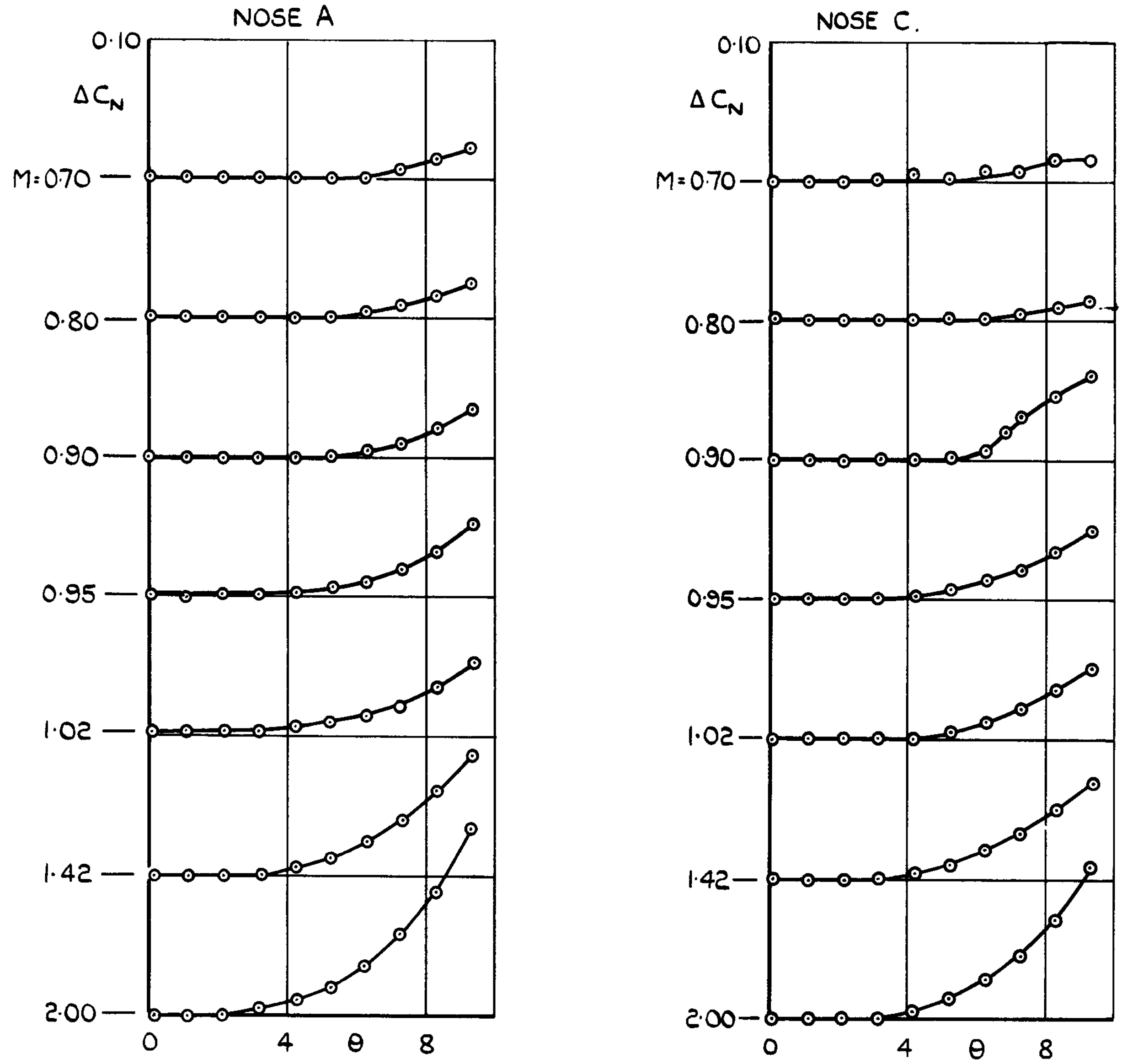

FIG. 9. VARIATION OF ΔC_N WITH θ FOR NOSES A AND C.

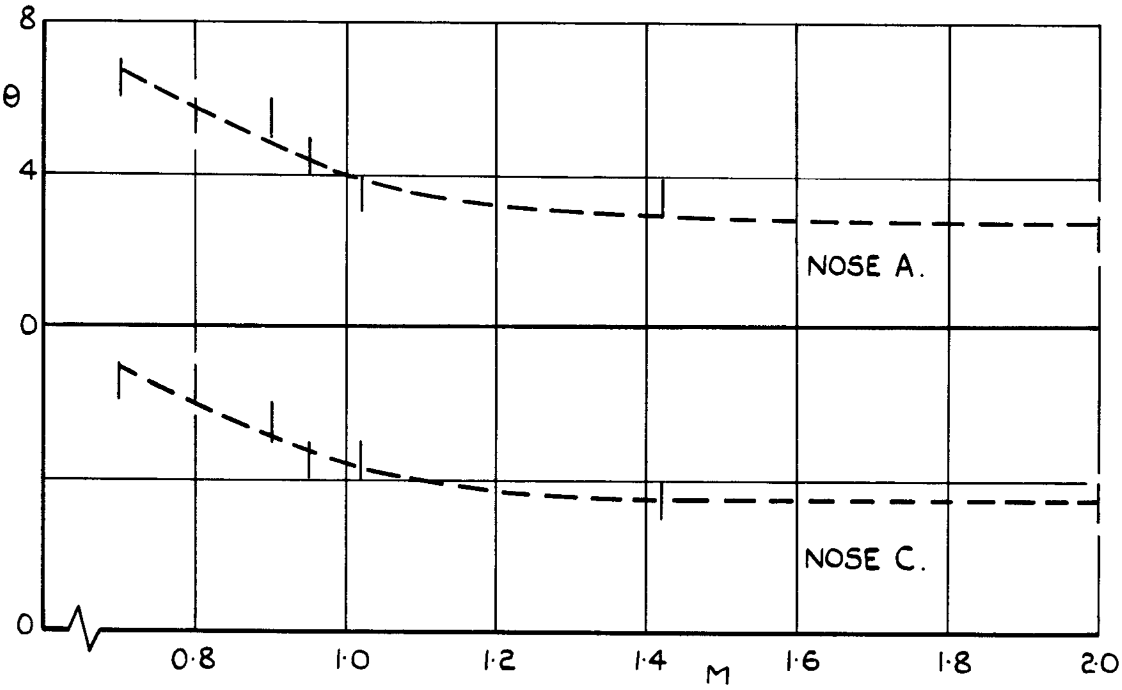

FIG. 10. VARIATION WITH MACH NUMBER OF INCIDENCE AT WHICH NON-LINEAR LIFT COMMENCES.

Published by
HER MAJESTY'S STATIONERY OFFICE

To be purchased from
York House, Kingsway, London w.c.2
423 Oxford Street, London w.1
13A Castle Street, Edinburgh 2
109 St. Mary Street, Cardiff
39 King Street, Manchester 2
Tower Lane, Bristol 1
2 Edmund Street, Birmingham 3
80 Chichester Street, Belfast 1
or through any bookseller

Printed in England

S.O. Code No. 23-9012-7